Investigation of defect recovery in deformed Pd; correlation between positron lifetime, enhanced hydrogen solubility, and transmission electron microscopy analysis

Hyunsu Ju and Brent J. Heuser *
Department of Nuclear, Plasma, and Radiological Engineering, University of Illinois, Urbana, Illinois 61801

and

Dallas R. Trinkle, Virginia McCreary, Jamey A. Fenske, and Ian M. Robertson
Department of Materials Science and Engineering, University of Illinois, Urbana, Illinois 61801

* Corresponding Author. Tel.: +1 (217) 333-9610; Fax.: +1 (217) 333-2906
Electronic mail: bheuser@illinois.edu

Abstract
Measurements of positron lifetime and hydrogen solubility were made in deformed polycrystalline Pd to investigate thermally-activated recovery. A strong correlation as a function of isochronal annealing temperature was observed between trapped-positron lifetime and the enhancement of hydrogen solubility due to solute binding at dislocations. This correlation is attributed to the simultaneous recovery of di-vacancies and dislocations versus annealing temperature. First principles calculations of positron lifetime at various defects in Pd support this conclusion. *In situ* transmission electron microscopy analysis demonstrates that significant dislocation recovery occurs between 450 and 600K in deformed polycrystalline Pd, and that low-angle tilt boundaries form above ~600K that persist to ~800K.

Keywords: DFT, positron, palladium, dislocation, vacancy, hydrogen, recovery, TEM

1. Introduction

Positron annihilation lifetime spectroscopy (PALS) is a well-established technique for investigating the open-volume defects in solids, such as vacancies in crystalline metals [1, 2]. Positron annihilation studies of hydrogen-induced defects in Nb [3, 4] and Pd [5, 6] have been recently performed. Generally, an increase in the mean positron lifetime, defined as an intensity-weighted combination of two or three lifetime components, is observed after hydrogen loading and unloading. This increase is attributed to positron trapping at vacancies, the creation of which is associated with the plastic deformation accompanying hydride formation and decomposition. Sakaki *et al*. [6] monitored the recovery process in deformed Pd with PALS. These authors induced plastic deformation by Pd hydride formation and decomposition at room temperature, a process known to generate significant dislocation density [7, 8]. A continuous reduction in the mean lifetime was observed during isochronal annealing between 323 and 1073 K that was attributed to vacancy recovery [6].

We have performed PALS measurements of defect recovery in deformed polycrystalline Pd, similar to the work of Sakaki *et al.*, and observed a comparable trend with respect to isochronal annealing temperature. We have in addition monitored the hydrogen solubility enhancement ratio, which is a direct measure of the hydrogen-dislocation trapping interaction [9-11]. The strong correlation we observed between the solubility enhancement ratio and trapped-positron lifetime demonstrates that dislocation and vacancy recovery track together with respect to annealing temperature. We also present first principles density functional theory calculations of positron lifetime at various relaxed sites in Pd, including an edge dislocation, a vacancy, and a di-vacancy. These results allow us to attribute the measured positron lifetime in deformed Pd to di-vacancy trapping. Finally, we track the evolution of the dislocation substructure with temperature in deformed polycrystalline Pd using transmission electron microscopy (TEM) and find supporting evidence for our conclusions regarding defect recovery.

2. Experimental

Polycrystalline Pd sheet purchased from Alpha Aesar was used for the experiments presented here. This sheet was 0.25 mm thick, cold-rolled in the as-received condition, and had a purity of 99.98%. Two identical 1 x 1 cm^2 samples cut from this sheet were used for both the PALS and hydrogen solubility measurements. The total mass of the two samples was 1.0523 grams. All sample surfaces were mechanically abraded with fine-grit paper and ultrasonically cleaned with alcohol-based solvents. No attempt was made to remove the native oxide that formed after this cleaning. However, the thermalization depth of positrons from the decay of ^{22}Na (see below) is 50 to 100 μm in most metals [2, 12]. The PALS technique is therefore considered a bulk probe, largely insensitive to surface oxide when high-energy positrons are used. The samples were then abraded, ultrasonically cleaned, and annealed in vacuum at 1173 K for 2.5 hours to induce recrystallization. A PALS measurement was performed after this initial annealing prior to deformation. The polycrystalline samples were deformed by cycled across the hydride miscibility gap twice at room temperature. Cycling was performed by exposure to hydrogen gas at pressures up to approximately 1 atm., followed by hydrogen desorption under vacuum. Isochronal annealing, beginning at 273 K and ending at 1173 K, was performed in vacuum for 2.5 hours at each annealing step. The positron lifetime spectrum and hydrogen solubility were both measured at room temperature after each annealing step. In addition to the polycrystalline samples, a PALS measurement of two identical, 1.0 cm diameter, 2 mm thick, well-annealed, single crystal Pd samples was performed at room temperature. The single crystal sample surfaces were mechanically polished to 0.05

μm with gamma alumina. The single crystal PALS measurements serve as a benchmark reference.

Hydrogen solubility measurements were performed by measuring two quantities related to the absorption of hydrogen gas by the polycrystalline samples in a closed volume, the total pressure change and final equilibrium pressure. The total hydrogen concentration can be determined from the total pressure change using the sample mass, system volume, and the ideal gas law. The bulk hydrogen concentration is determined from the equilibrium pressure using Sieverts' law constants for Pd [13]. The difference between the total and bulk hydrogen concentration is the excess hydrogen concentration trapped at defects [7, 8]. The ratio of total-to-bulk hydrogen concentration, α, is known as the solubility enhancement ratio and is typically between 1.2 and 1.4 for cold rolled or cycled Pd when measured at bulk concentrations of approximately 0.005 [H]/[Pd] [7-11]. Solubility enhancement ratios in excess of this range (α~1.6) have been observed by Flanagan *et al.* [10] in heavily cold worked Pd and by us here after hydride cycling.

Positron lifetime spectra were measured with an AMETEC-ORTEC system comprised of two 905-21 fast plastic scintillator detectors and associated fast coincidence counting channels. This system had a 92 ps resolution standard deviation as determined by the manufacturer. A 10 mCi ^{22}Na source encapsulated in Ni foil was used for the PALS measurements. ^{22}Na emits a broad continuum of positrons with end-point energy 545 keV and average energy 215 keV. High-energy positrons annihilate with electrons after thermalization to the sub-eV energy range. The associated penetration depth (e-folding depth) is approximately 20 μm in Pd [2, 12]—thus we consider PALS with a ^{22}Na source to be a bulk characterization technique of defects in Pd. PALS measurements require two identical samples that sandwich the source. This ensures that the majority of positrons emitted by the source annihilate in either of the two identical samples.

In situ TEM analysis was performed using a JEOL 2010 microscope, which is equipped with a LaB_6 source and was operated at an accelerating voltage of 200kV. The deformed polycrystalline Pd specimen was fabricated from the same material used for PALS analysis and the hydrogen solubility measurements. The TEM specimen was first dimpled with 3 μm diamond paste and then ion milled to produce usable thin area with a Fischione Ion Mill. Ion milling was performed with the specimen actively cooled with liquid nitrogen to prevent annealing and associated dislocation recovery. Ion milling is known to introduce lattice damage; this damage was observed in TEM analysis and discussed below with regard to the temperature-dependent dislocation recovery process.

3. Results and discussion

Two representative convoluted decay spectra, $N(t)$, of the polycrystalline Pd samples, the post-deformation/pre-anneal and the post-deformation/post-1173K-anneal, are shown in Figure 1. These spectra were fit with a three-component positron lifetime spectrum convoluted with a Gaussian resolution function. This convolution is given by,

$$N(t) = \sum_{i=1}^{3} \frac{I_i}{2} \exp\left[\frac{\left(t - t_o - \sigma^2/4\tau_i\right)}{\tau_i} \right] \times \left[1 - \mathrm{erf}\left(\frac{\sigma}{2\tau_i} - \frac{t - t_o}{\sigma} \right) \right], \qquad [1]$$

where I_i and τ_i are the relative intensity and positron lifetime, respectively, of the i^{th} component, σ is the

standard deviation of the resolution function, and t_o is the timing delay. A constant background term was included in each fit as well. The only constraint placed on the fit was $\tau_i > 80$ ps. The timing delay is a standard feature of the PALS measurement technique and is introduced in the annihilation-γ counting channel to shift the time measurement to the linear operating regime of the time-to-analog converter. Although $\sigma = 92$ ps was quoted by the manufacturer, we found $\sigma = 140$ ps to be more representative of our measured spectra from the data fits. Attempts to use $\sigma \sim 90$ ps resulted in much poorer fits in general.

The two dominant components of the measured decay spectra, the i=1 and i=2 components, are plotted as a function of post-deformation annealing temperature in Figs. 2 and 3. These components are identified with the bulk positron lifetime in Pd and with positrons trapped at di-vacancies, respectively, as discussed below. The minor i=3 component, also shown in Figs. 2 and 3, comprised a very small fraction of the total intensity ($I_3 \sim 10^{-2}$, Fig. 2) with a lifetime of order $\tau_3 \sim 300$ ps (Fig. 3) over most of the annealing temperature range. Long-lived positron trapping modes ($\tau \sim 300$ ps) observed in Pd have been attributed to large-angle grain boundaries [14] and this explanation may be valid in our polycrystalline samples as well. The shift of relative intensity from the trapping I_2 component ($\tau_2 \sim 170$ ps) to the bulk I_1 component ($\tau_1 \sim 90$ ps) versus annealing temperature is consistent with the elimination of positron trapping defects during the recovery process. This is discussed in more detail below. The I_1 and I_2 intensity components of the polycrystalline samples shown in Fig. 2 level off above 950 K to values similar, but not equal, to those measured for the well-annealed single crystal sample. This is likely an inherent difference between the two sample matrices and may be due to the persistence of open volume defects in the polycrystalline sample material.

Density-functional theory (DFT) for electrons and positrons can be used to calculate the positron ground-state wavefunctions at different defect trap sites in Pd. The seven structures considered here—fcc Pd, Pd vacancy in a 4x4x4 cubic supercell (0.4% atomic concentration), Pd di-vacancy in a 4x4x4 cubic supercell, H interstitial in a 4x4x4 cubic supercell (0.4% atomic concentration), quasi-random $Pd_{108}H_{68}$ in a 3x3x3 cubic supercell (63% atomic concentration), edge dislocation [15], and edge dislocation with H interstitial in partial core [15]—were first relaxed to their minimum energy atomic positions using VASP [16, 17] with PAW potentials [18] in the LDA [19]. This treatment, with planewave cutoff energies of 250 eV, produces lattice constants, elastic moduli, phonon spectra for Pd, H dimer distances and H octahedral versus tetrahedral site energy differences in good agreement with experiment. Using the total electron charge density on a real space grid along with the ionic potentials with the Boronski and Nieminen local-density approximation for the positron/electron correlation [20], the ground state wavefunction was calculated for the positron on the same grid as the charge density. The convolution of the positron probability density with the electron charge density and an enhancement factor gives the expected lifetime of the positron [20]. Examples of the ground-state positron wavefunction associated with a mono-vacancy and a di-vacancy in Pd are shown in Figure 4. The positron wavefunction is enhanced in regions of low electron density, leading to greater lifetimes. The calculated positron lifetime values τ_C in Pd are shown in Table 1. In addition, the measured lifetimes corresponding to the I_i components and the single crystal sample are listed in Table 1.

Several aspects of the DFT calculations are noteworthy. First, the bulk value, $\tau_C = 98.5$ ps, is consistent with our measured I_1 component lifetime ($\tau_1 \sim 90$ ps), as well as being in agreement with the work of Robles *et al.* for the LDA [21]. This τ_C value is also in very good agreement with the bulk lifetime we recorded with the single crystal samples ($\tau_1 = 97$ ps). The effect of adding a single interstitial hydrogen atom to Pd (Int. H in α-$PdH_{0.004}$ in Table 1) is negligible. This is expected since the

positron wavefunction simply avoids the interstitial site occupied by the hydrogen atom in the dilute α-Pd phase. Second, the positron lifetime is increased only slightly in disordered α' hydride phase. More importantly, the positron lifetime is largely unaffected by the presence of an edge dislocation (split into partials [15]) in Pd. This is because the tensile strains associated with the two partials are small; the effect is a very slight (~2%) increase in τ_C relative to the bulk Pd lifetime. As expected, the effect of adding an interstitial hydrogen atom to the dislocation simulation cell (a single hydrogen atom was placed at the core of one partial) is insignificant. Finally, the positron lifetime increases significantly when a single vacancy (mono-vacancy case in Table 1) and a two-vacancy cluster (di-vacancy case in Table 1) are added to the perfect Pd simulation cell. The rationale behind our connection of the measured I_2/τ_2 component to positron trapping at di-vacancies is two-fold. First, the general agreement between the two lifetimes, τ_C = 154 ps and τ_2 ~ 170 ps, supports this choice. Second, the appreciable increase in τ_C when a second vacancy is added to create a di-vacancy complex implies a vacancy cluster (of at least two vacancies) is responsible for the observed τ_2 trapped component. We mention here that others have calculated the positron lifetimes at mono- and di-vacancies in Pd, finding values similar to or greater than our DFT results [5, 21]. Thus, while our DFT results suggest the measured I_2/τ_2 component is due to positron trapping at di-vacancies, it does not constitute proof. Rather, the preponderance of the evidence, presented here and by others elsewhere, indicates that the I_2/τ_2 component is likely to due positron trapping at open-volume defects (di-vacancies or perhaps larger vacancy clusters) induced by the hydride cycling deformation procedure.

As stated above, we have measured the hydrogen solubility enhancement ratio α for the polycrystalline samples as a function of annealing temperature. The dependence of both α and I_2 (the latter normalized to one at T=1173 K) on the annealing temperature is shown in Figure 5. These data demonstrate that dislocation recovery, as monitored by α, and the recovery vacancy clusters, as monitored by I_2, track together with the annealing temperature. This is expected in general since dislocation motion during dislocation recovery will eliminate point defects, as will thermally-driven migration to sinks. Saturated vacancy-cluster recovery (invariant I_2 above 950 K) is offset by ~200 K relative to the termination of dislocation recovery (invariant behavior above ~750K) in Figure 5. This is discussed presently.

TEM analysis of *in situ* dislocation recovery is shown in Figure 6. The four micrographs shown represent the equilibrium dislocation substructure at each temperature. Typically several minutes were required at each temperature for the specimen to reach equilibrium with respect to dislocation motion and recovery. At low temperatures, below ~450K, the most significant change was the loss of ion milling damage, presumably dislocation loops created by ion bombardment associated with the milling process. The presence of the milling damage may have delayed the onset of dislocation recovery. However, the purpose of TEM analysis was not to establish the exact temperatures associated with dislocation recovery steps, but rather to confirm that significant recovery occurs between ~450 and ~650K, consistent with the trend in α in Figure 5.

The most important observations from TEM analysis are 1) that significant dislocation recovery does occurs between 450 and 650K and 2) that this recovery is associated with the formation of low-angle tilt boundaries, which then become the dominate dislocation substructure feature that persists to T~800K (the upper temperature limit of TEM analysis). The dislocation trapping interaction, as monitored by the hydrogen solubility measurements, indicates that dislocation recovery is essentially complete at 700K. This corresponds to the evolution of the dislocation substructure observed with TEM; in particular

recovery over a similar temperature range, which then leads to stable low-angle dislocation tilt boundaries. The temperature associated with the formation of stable low-angle tilt boundaries (600~650K) corresponds to relatively low measured hydrogen solubility enhancement (α~1.1). Therefore, the nearly complete dislocation recovery below 650K observed with TEM is consistent with α~1, provided the low-angle tilt boundaries do not result in enhanced dislocation solubility. We believe this is the case since large-angle grain boundaries, which will have greater local tensile strain compared to low-angle tilt boundaries and therefore more strongly trap hydrogen, do not result in measureable enhanced hydrogen solubility [7, 9, 10].

As stated above, the recovery of vacancy clusters monitored with PALS is shifted by ~200K to higher temperature compared to dislocation recovery. We attribute this to higher migration and/or dissociation enthalpy of the di-vacancy complex. In addition, the formation of stable tilt boundaries arrests the dislocation recovery (at least below 800K), rendering this process ineffective with respect to further vacancy recovery.

Vacancy recovery has been studied in a variety of materials for several years using resistivity measurements [22-29], and more recently with PALS [6, 30]. Generally, point defect recovery as characterized by resistivity changes with temperature is divided into four stages, with stage IV (T>500K) attributed to the dissociation or migration of vacancy clusters that form during stage III [25, 29]. Schilling and Sonnenberg also include the possibility of a di-vacancy contribution to stage III recovery based on observed activation enthalpies in irradiated metals [22]. As discussed above, the τ_2 trapping component is attributed to di-vacancies (or larger) clusters. We observe complete recovery of this trapping component only above 900K. The work of Nakagawa *et al*. [24] includes neutron-irradiated Pd, which tracts point defect recovery via resistivity between 20K and 400K. Recovery in Pd was ~70% complete at 300K and ~90% complete at 400K, the temperature range they attribute to stage III recovery. Their result does not exclude further recovery that could be attributed to stage IV in Pd, beyond ~400K. Furthermore, if stage III recovery is responsible for vacancy cluster formation that leads to stage IV recovery, then the termination of stage III at 400K in Pd is consistent with our observed trend in τ_2, which will be dominated by stage IV recovery. The reason for this statement is that our isochronal annealing procedure was not sensitive to stage III since we did not attempt to resolve changes on a fine enough temperature scale below 400K.

Finally, the work of Arunkumar *et al*. [30] is noteworthy within the current discussion. These authors monitored defect recovery in proton-irradiated a stainless steel alloy with PALS and observed a ~165 ps trapping component that recovered to the bulk un-irradiated value (108 ps) between 300 and 700K [30]; in other words, a very similar trapped lifetime and temperature trend we report here. Arunkumar *et al*. attributed this lifetime component to “vacancy-defect” trapping, but did not specify the nature of the vacancy defects (mono-vacancies versus vacancy clusters). Our DFT calculations indicate that this trapping component, at least in Pd, is due to di-vacancy trapping.

4. Summary

We have monitored the defect recovery process in deformed polycrystalline Pd with positron annihilation lifetime spectroscopy, in hydrogen solubility measurements, and with TEM analysis. The following statements summarize this work:

1. The recovery of dislocations and open-volume defects (di-vacancies and vacancy clusters) in polycrystalline Pd proceed together during isochronal annealing. However, the recovery of the latter is shifted by ~200 K compared to the former. This is attributed to the stabilization of the dislocation substructure and the formation of low-angle tilt boundaries mitigating the sensitivity of the hydrogen solubility measurements. In addition, the formation of these boundaries eliminates dislocation recovery as a viable mechanism for further vacancy cluster recovery. Vacancy cluster recovery is then dictated by higher migration and/or dissociation enthalpy associated with stage IV vacancy recovery.

2. DFT calculations support the hypothesis that the two primary components of the positron decay spectra observed here are due to positron annihilation in defect-free bulk Pd and to positron trapping at di-vacancies. The effect of edge dislocations, split into two partials, on the positron lifetime is insignificant.

3. Comparison of the post-deformation/post-anneal polycrystalline positron decay spectrum to that of the well-annealed single crystal, which to the best of our knowledge does not exist in the published literature, indicates the possible influence of post-recovery positron trapping in the polycrystalline matrix. We suspect this is an inherent difference between the two different matrices and may be an indication of the persistence of open volume defects in the polycrystalline material.

4. *In situ* TEM analysis confirms the temperature dependence of dislocation recovery observed in hydrogen solubility measurements. This analysis also reveals the formation of stable low-angle tilt boundaries above ~600K, which are not expected to trap measurable quantities of hydrogen.

Acknowledgement

This work was supported by the NSF under Grant Number DMR-0804810. The TEM work performed by IMR, JAF, and VC was supported by the U.S. DOE Office of Basics Sciences as part of the Center for Defect Physics under Award Number DE-AC05-00OR22715. In addition, this work was carried out in part in the Frederick Seitz Materials Research Laboratory Central Facilities, University of Illinois, which are partially supported by the U.S. Department of Energy under grants DE-FG02-07ER46453 and DE-FG02-07ER46471.

Bibliography

1. I.K. MacKenzie, T.L. Khoo, A.B. McDonald, and B.T.A. McKee, Phys. Rev. Lett., V19 (1967) 946.
2. M.J. Puska and R.M. Nieminen, Rev. Mod. Phys., V66 (1994) 841.
3. J. Cizek, I. Prochazka, S. Danis, M. Cieslar, G. Brauer, W. Anwand, R. Kirchheim, and A. Pundt, J. Alloys Compounds, V446-447 (2007) 479.
4. J. Cizek, I. Prochazka, F. Becvar, R. Kuzel, M. Cieslar, G. Brauer, W. Anwand, R. Kirchheim, and A. Pundt, Phys. Rev. B, V69 (2004) 224106.
5. M. Mizuno, R. Tonomori, Sakaki, H. Araki, and Y. Shirai, Sol. State Ionics, V172 (2004) 149.
6. K. Sakaki, M. Mizuno, H. Araki, and Y. Shirai, J. Alloys Compds, V414 (2006) 204.
7. B.J. Heuser, J.S. King, G.C. Summerfield, F. Boue, and J.E. Epperson., Acta Metall. Mat., V39 (1991) 2815.
8. B.J. Heuser and J.S. King, J. Alloys and Compounds, V261 (1997) 225.
9. T.B. Flanagan and J.F. Lynch, J. Less-Common Metals, V49 (1976) 25.
10. T.B. Flanagan, J.F. Lynch, J.D. Clewley, and B. Von Turkovich, J. Less-Common Metals, V49 (1976) 13.
11. R. Kirchheim, Acta Metallurgica, V29 (1981) 835.
12. W. Brandt and R. Paulin, Phys. Rev. B, V15 (1977) 2511.
13. F. Fromm and H. Jehn, Bull. Alloy Phase Dia., V5 (1984) 325.
14. T.E.M. Staab, R. Krause-Rehberg, and B. Kieback, J. Mat. Sci., V34 (1994) 3833.
15. B.J. Heuser, H. Ju, D.R. Trinkle, and T.J. Udovic, *Effects of Hydrogen on Materials*, Proc. 2008 Int. Hydrogen Conf., Eds. B. Somerday, P. Sofronis, and R. Jones, 2009 ASM Int., p464.
16. G. Kresse and J. Hafner, Phys. Rev. B **47**, 558 (1993).
17. G. Kresse and J. Furthmuller, Phys. Rev. B **54**, 11169 (1996).
18. G. Kresse and J. Joubert, Phys. Rev. B **59**, 1758 (1999).
19. J. P. Perdew and Alex Zunger, Phys. Rev. B **23**, 5048 (1981).
20. E. Boronski and R. M. Nieminen, Phys. Rev. B **34**, 3820 (1986).
21. J.M. Robles, E. Ogando, and F. Plazaola, J. Phys.: Condens. Matter **19**, 176222 (2007).
22. W. Schilling and K. Sonnenberg, J. Phys. F: Metal Phys. **3**, 322 (1973).
23. L. Stals, J. Nihoul, J. Cornelis, and P. De Meester, Phys. Stat. Sol. **18**, 283 (1973).
24. N. Nakagawa, K. Boning, P. Rosner, and G. Vogl, Phys. Rev. B **16**, 5285 (1977).
25. S. Takaki, J. Fuss, H. Kugler, U. Dedek, and H. Schultz, Radiat. Effs. **79**, 87 (1983).

26. C. Dimitrov, B. Sitaud, X. Zhang. O. Dimitrov, U. Dedek, and F. Dworschak, J. Phys.: Condens. Matter **4**, 10211 (1992).
27. A.L. Nikolaev. V.L. Arbuzov, and A.E. Davletshin, , J. Phys.: Condens. Matter **9**, 4385 (1997).
28. G. Sattonnay, F. Ma, C. Dimitrov, and O. Dimitrov, , J. Phys.: Condens. Matter **9**, 5527 (1997).
29. C.-C. Fu, J. Dalla Torre, F. Willaime, J.-L. Bocquet, and A. Barbu, Nat. Materials **4**, 68 (2005).
30. J. Arunkumar, S. Abhaya, R. Rajaraman, G. Amarendra, K.G.M. Nair, C.S. Sundar, B. Raj, J. Nucl. Mater. **384**, 245 (2009).

Table 1. Calculated and measured positron lifetimes.

Defect/Sample/Component	τ_C / τ_i [ps]
Bulk Pd	98.5
Int. H in α–Pd	98.5
$PdH_{0.63}$ (α' phase)	100.1
Dislocation in Pd	100.3
Dislocation in Pd + Int. H	100.2
Mono-vacancy in Pd	134
Di-vacancy in Pd	154
I_1 (bulk, single crystal Pd)	97
I_1 (bulk, polycrystalline Pd)	~90
I_2 (vacancy cluster)	~170
I_3 (open-vol., grain boundary)	~300

Figure Captions

Figure 1. Positron convoluted decay spectra for the post-deformation/pre-anneal polycrystalline Pd samples (open boxes) and for the post-deformation/post-900°C-anneal (that is, after the last step in the isochronal annealing procedure) polycrystalline sample (open circles). The solid lines are best fits using Equation. 1. The data sets have been offset vertically for clarity. The peak of each spectrum does not correspond to t=0 because of the t_o delay discussed in the text.

Figure 2. Polycrystalline Pd fractional lifetime intensity versus annealing temperature for the two dominate components of the positron decay spectrum, I_1 (open circles, τ_1~90 ps) and I_2 (solid boxes, τ_2~170 ps), corresponding to bulk Pd and di-vacancy trapping, respectively. The minor component, I_3 (solid triangles, τ_2~300 ps), attributed to grain boundary trapping (see text) is also shown multiplied by a factor of four. The shift of intensity between the primary components, from I_2 to I_1, is consistent with a reduction of di-vacancy trapping sites with annealing temperature and therefore recovery. The I_1 and I_2 intensity fractions for as-received sample after initial annealing are shown as upper and lower vertical lines, respectively, on the left side of the figure. The I_1 and I_2 intensity fractions for well-annealed single crystal Pd are shown as upper and lower vertical lines, respectively, on the right side of the figure.

Figure 3. Positron lifetimes for polycrystalline Pd versus annealing temperature for τ_1 (open circles), τ_2 (solid boxes) τ_3 and (solid triangles). The trapped-positron lifetime τ_2 is invariant with respect to annealing temperature, consistent with notion that the trapping defect size does not change during recovery. The corresponding bulk lifetime for the single crystal Pd samples is τ_1=97 ps (not shown).

Figure 4. The positron groundstate wavefunction near a Pd vacancy (a) and divacancy (b) on the (100) plane. The positron is attracted to regions of lower electron potential, away from the ionic cores. Moreover, a smaller overlap with electron density produces a longer lifetime. In the case of the divacancy compared with the vacancy, the positron spreads out primarily in the region between the two neighboring vacancies, which has a lower electron density.

Figure 5. Correlation in polycrystalline Pd between enhanced hydrogen solubility, α (solid boxes), and relative intensity of the trapped component, I_2 (open circles), normalized to one at T=1173 K. The solubility enhancement ratio is normalized to one at full dislocation recovery by definition. These two quantities track together with an offset to higher temperature (~200 K) for vacancy recovery.

Figure 6. TEM analysis of *in situ* dislocation recovery versus temperature. The images represent the same analysis area after a holding time of several minutes at the temperatures shown to allow for equilibrium with respect to dislocation substructure evolution. Above approximately 600K the dislocation substructure consists almost entirely of stable low-angle tilt boundaries that are not expected to influence the measured hydrogen solubility enhancement ratio. The markers show two locations where low-angle dislocation tilt boundaries form: 473K—boundaries not yet formed; 536K—boundaries just becoming organized; 619K—stable boundaries formed; 773K—boundaries persist.

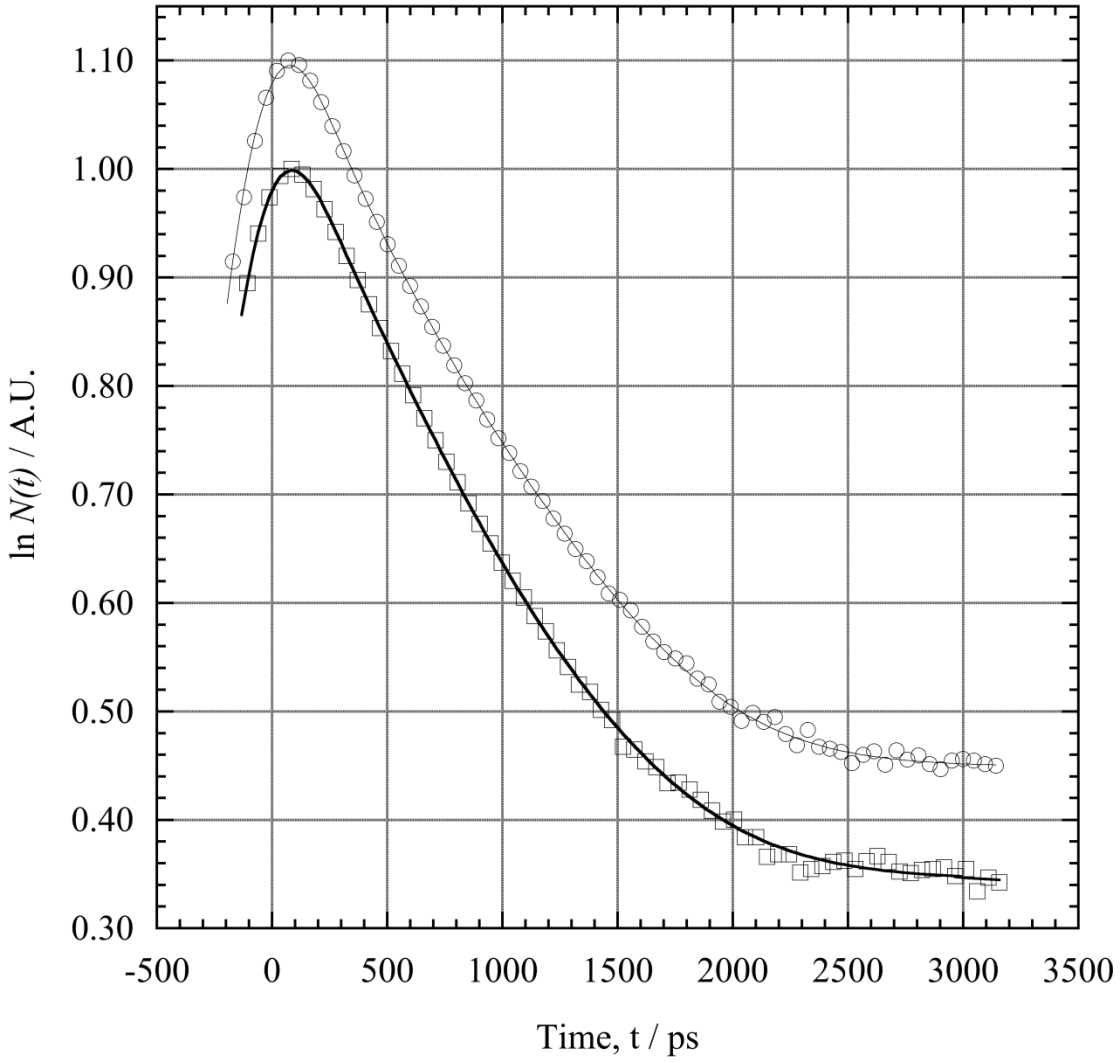

Figure 1. Ju *et al.*

Figure 1. Positron convoluted decay spectra for the post-deformation/pre-anneal polycrystalline Pd samples (open boxes) and for the post-deformation/post-900°C-anneal (that is, after the last step in the isochronal annealing procedure) polycrystalline sample (open circles). The solid lines are best fits using Equation. 1. The data sets have been offset vertically for clarity. The peak of each spectrum does not correspond to t=0 because of the t_o delay discussed in the text.

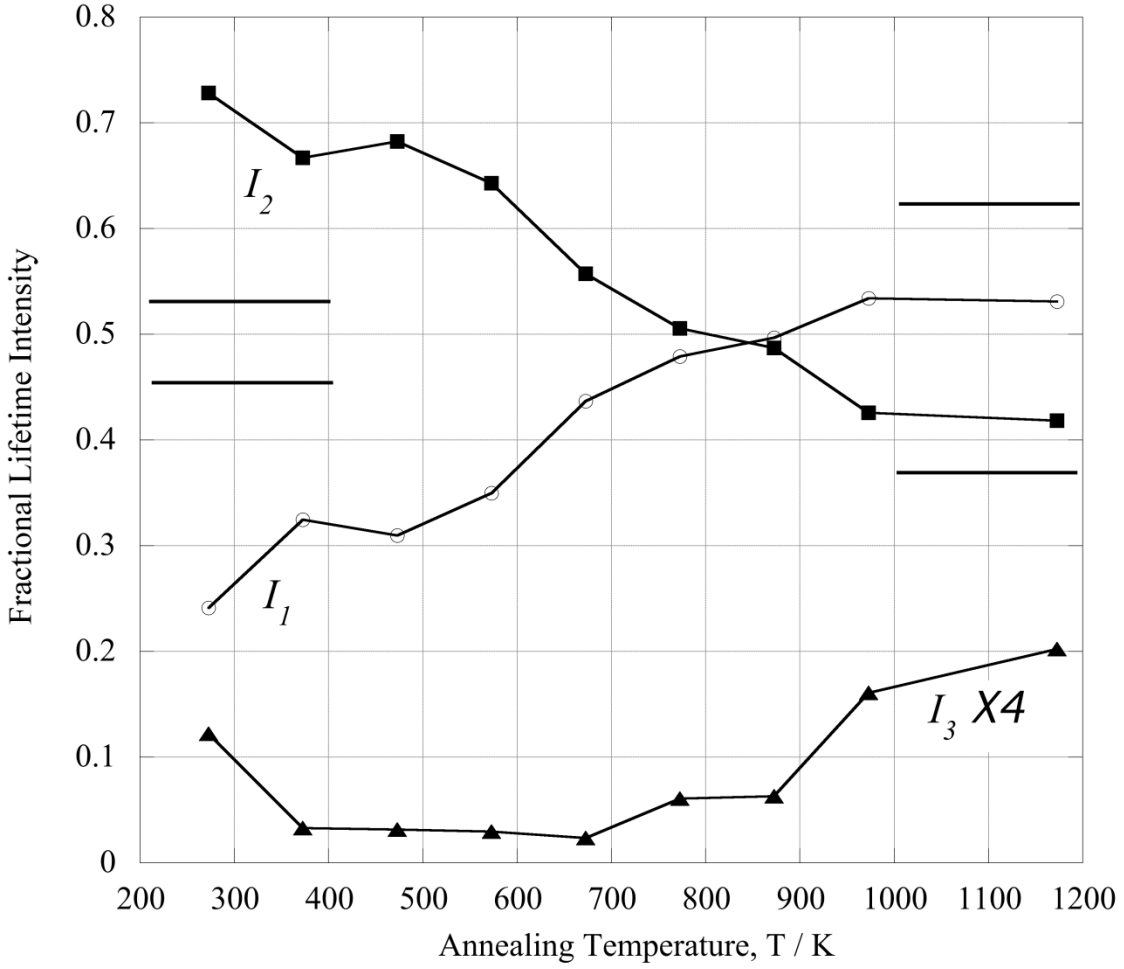

Figure 2. Ju *et al.*

Figure 2. Polycrystalline Pd fractional lifetime intensity versus annealing temperature for the two dominate components of the positron decay spectrum, I_1 (open circles, τ_1~90 ps) and I_2 (solid boxes, τ_2~170 ps), corresponding to bulk Pd and di-vacancy trapping, respectively. The minor component, I_3 (solid triangles, τ_2~300 ps), attributed to grain boundary trapping (see text) is also shown multiplied by a factor of four. The shift of intensity between the primary components, from I_2 to I_1, is consistent with a reduction of di-vacancy trapping sites with annealing temperature and therefore recovery. The I_1 and I_2 intensity fractions for as-received sample after initial annealing are shown as upper and lower vertical lines, respectively, on the left side of the figure. The I_1 and I_2 intensity fractions for well-annealed single crystal Pd are shown as upper and lower vertical lines, respectively, on the right side of the figure.

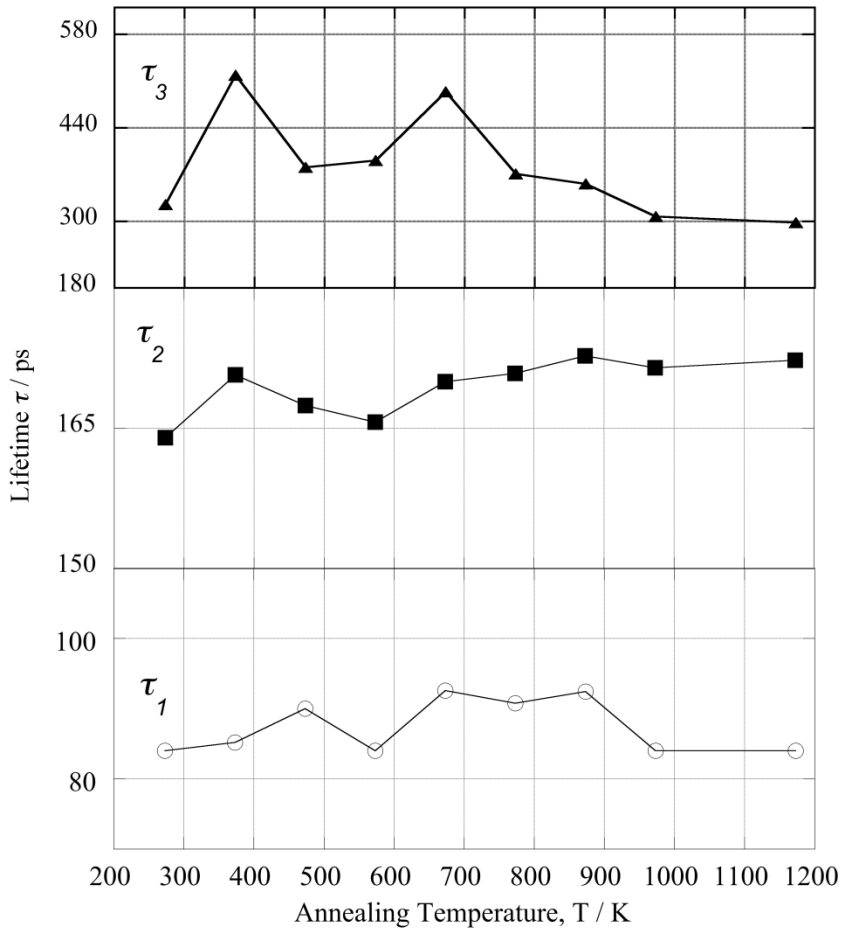

Figure 3. Ju *et al.*

Figure 3. Positron lifetimes for polycrystalline Pd versus annealing temperature for τ_1 (open circles), τ_2 (solid boxes) τ_3 and (solid triangles). The trapped-positron lifetime τ_2 is invariant with respect to annealing temperature, consistent with notion that the trapping defect size does not change during recovery. The corresponding bulk lifetime for the single crystal Pd samples is τ_1=97 ps (not shown).

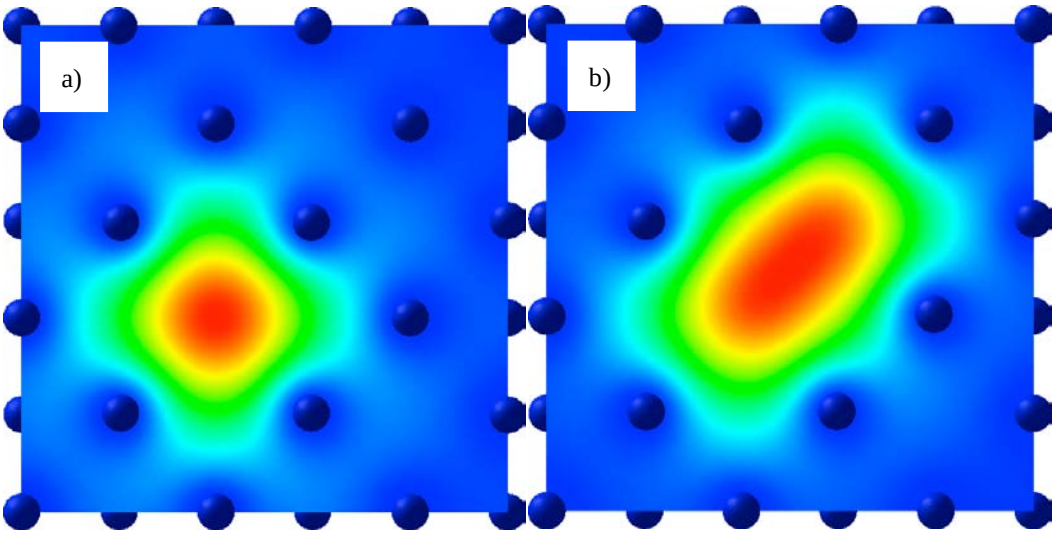

Figure 4. Ju *et al.*

Figure 4. The positron groundstate wavefunction near a Pd vacancy (a) and di-vacancy (b) on the (100) plane. The positron is attracted to regions of lower electron potential, away from the ionic cores. Moreover, a smaller overlap with electron density produces a longer lifetime. In the case of the di-vacancy compared with the vacancy, the positron spreads out primarily in the region between the two neighboring vacancies, which has a lower electron density.

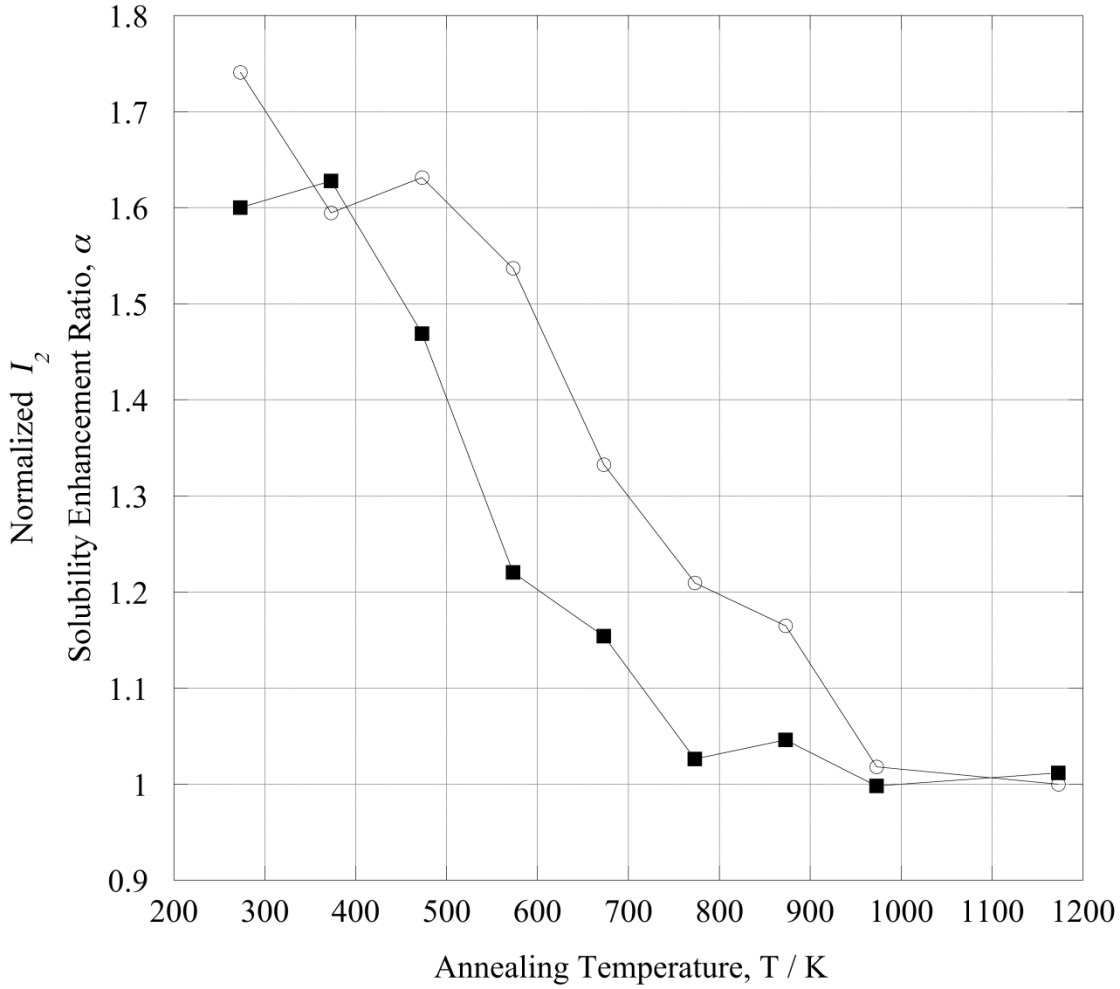

Figure 5. Ju *et al.*

Figure 5. Correlation in polycrystalline Pd between enhanced hydrogen solubility, α (solid boxes), and relative intensity of the trapped component, I_2 (open circles), normalized to one at T=1173 K. The solubility enhancement ratio is normalized to one at full dislocation recovery by definition. These two quantities track together with an offset to higher temperature (~200 K) for vacancy recovery.

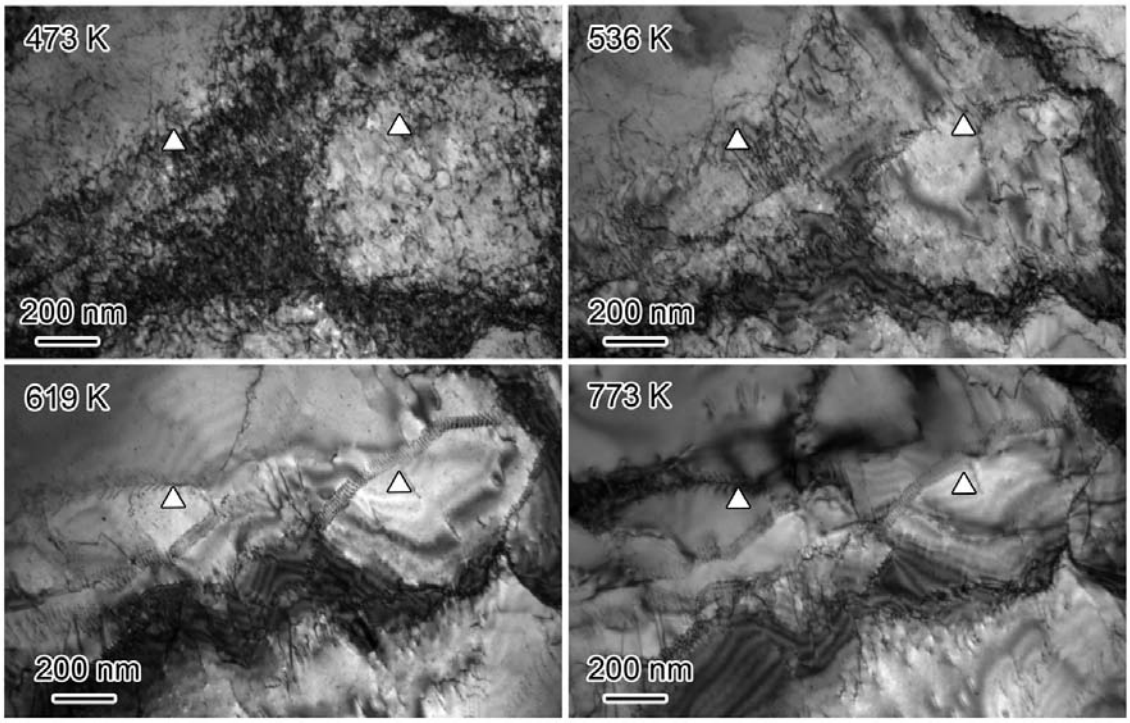

Figure 6. Ju *et al.*

Figure 6. TEM analysis of *in situ* dislocation recovery versus temperature. The images represent the same analysis area after a holding time of several minutes at the temperatures shown to allow for equilibrium with respect to dislocation substructure evolution. Above approximately 600K the dislocation substructure consists almost entirely of stable low-angle tilt boundaries that are not expected to influence the measured hydrogen solubility enhancement ratio. The markers show two locations where low-angle dislocation tilt boundaries form: 473K—boundaries not yet formed; 536K—boundaries just becoming organized; 619K—stable boundaries formed; 773K—boundaries persist.